Journal of Computational Applied Mechanics 2024, 55(-): PP-PP

DOI: 10.22059/JCAMECH.2024.375018.1040

RESEARCH PAPER

Static Stability Analysis of FG Thick Plate Supported by Three Parameters Foundation under General Boundary Conditions

Abdeljalil Meksi [a] , Rabbab Bachir Bouiadjra [b,c], Samir Benyoucef [b], Abdelhakim Bouhadra [b, d *], Mohamed Bourada [b], Mofareh Hassan Ghazwani [e] and Abdelouahed Tounsi [b, f]

[a] *Department of Civil engineering, Faculty of architecture and civil engineering, University of sciences and Technology Mohamed Boudiaf, Oran 31000, Algeria*
[b] *Material and Hydrology Laboratory, Civil Engineering Department, Faculty of Technology, Djillali Liabes University, Sidi Bel Abbes 22000, Algeria*
[c] *Department of Civil Engineering, University Mustapha Stambouli of Mascara 29000, Algeria*
[d] *Department of Mechanical Engineering, Faculty of Science and Technology, Abbes Laghrour University, Khenchela 40000, Algeria*
[e] *Department of Mechanical Engineering, Faculty of Engineering, Jazan University, P.O Box 45124, Jazan, Kingdom of Saudia Arabia*
[f] *Department of Civil and Environmental Engineering, King Fahd University of Petroleum & Minerals, 31261 Dhahran, Eastern Province, Saudi Arabia*

Abstract

In this paper, an analytical solution for exploring the buckling characteristics of functionally graded (FG) plate is presented based on a quasi-3D shear deformation theory. It is considered that the plate is subjected to different types of in-plane compressive load. The FG plate is placed on three-parameter foundation Winkler-Pasternak-Kerr. The overall material properties of FG plate are assumed to be varied across the thickness and are estimated through the Voigt micromechanical model. The governing equations are obtained on the base of the quasi-3D deformation theory that contain undetermined integral forms and involves only four unknowns to derive. Equations of motion are derived from the principal of virtual work and the analytical solution is used to determine the critical buckling loads. By the discussion of numerical examples and the comparison with those of the reports in the literature, the convergence and the reliability of the present approach are validated. Finally, the parametric investigations of the in-plane buckling are carried out, including the influence of boundary conditions, elastic foundation, plate geometric parameters and power law index. The results reveal that the critical buckling loads are strongly influenced by several parameters such as boundary conditions, elastic foundation parameters and geometric shape of the plate.

Keywords: Mechanical Buckling, In-plane compressive load, plate, elastic foundation, boundary conditions;

* Corresponding author. Tel.: +213 777 189 718;
E-mail address: abdelhakim.bouhadra@univ-khenchela.dz

1. Introduction

Functionally graded materials (FGM) are inhomogeneous advanced composite materials that have been introduced into industry in recent years. They are made of a mixture of two or more distinct material phases generally ceramic and metal. The mechanical properties of these materials changes gradually in one (or more) direction(s) according to a specific function. Since these materials exhibit many desirable properties, they can be used as effective compositions for beams, plates and shells [1]. In the open literature, investigation of mechanical behavior of structures made from FGM have been widely reported and therefore many solutions and models were proposed [2-7]. Plates are important components in many engineering applications. They are used in several practical situations such ship buildings and automotive industry where these plates can be submitted to in-plane loads of different types that can cause buckling, a phenomenon which is highly undesirable. Therefore, knowledge of the stability characteristics of FG plates is of great practical importance for the design of plates. Consequently, several researchers have been interested in this research axis and several works have been published.

Sari et al. [8] used the classical plate theory (CPT) and the Eringen's nonlocal elasticity theory to study the buckling of FG thin nanoplate subjected to biaxial linearly varying mechanical loads and various temperature distributions through the thickness. Taczała et al. [9] studied the nonlinear stability of stiffened FG plates subjected to thermo-mechanical loading using the First Shear Deformation Theory (FSDT) in conjunction with finite element method (FE). Using the same theory, Thang et al. [10] obtained an approximate solution to study the elastic buckling and free vibration of porous-cellular plates. Chen et al. [11] proposed a new distribution of porosity to study the buckling of FG porous plates. They used the FSDT to determine the governing equations and then used the Chebyshev polynomials-based Ritz method to obtain the buckling loads. By the mean of the Third order Shear Deformable Theory (TSDT), Abdelrahman [12] analyzed the effect of transverse variation of material properties on the buckling of simply supported FG plates. In the same framework and in a conjunction with the nonlocal elasticity Eringen's model, Cutolo et al. [13] presented an analytical solution for the buckling and free vibrations analysis of thick FG nanoplates resting on Pasternak foundation. Van Do et al. [14] used the higher-order shear deformation theory (HSDT) and the mesh-free approximation based on the radial point interpolation method (RPIM) to predict the nonlinear post-buckling behavior of FG plates. Thinh et al. [15] analyzed the dynamic and the buckling behavior of FG plate using a higher order displacement field with twelve-unknown functions. Yi et al. [16] presented a closed-form solution based on a special higher-order shear and normal deformable plate theory for the static, dynamic and buckling analysis of a simply supported FG plates. Kar and Panda [17] examined analytically the post-buckling behaviour of FG curved shell panels with different geometries subjected to uniaxial and the biaxial edge compression. The authors used the HSDT in conjunction with Green-Lagrange geometrical nonlinear strains. Singh et al. [18] developed a semi-analytical solution based on HSDT with consideration of the von-Karman geometric nonlinearity to study dynamic buckling, dynamic response and shock spectrum of imperfect plate under various types of in-plane pulse forces. Kolakowski and Czechowski [19] studied linear and non-linear stability of a square in-plane FG plate made of a step-variable gradation material. Cong et al. [20] investigated the nonlinear buckling and post-buckling behavior of FG imperfect plates resting on Pasternak foundation exposed to mechanical, thermal and thermo-mechanical loads. They used the Reddy's higher-order shear deformation plate theory to formulate the problem and the Galerkin method to determine the buckling loads. Tamrabet et al. [21] developed a powerful method to analyze how porous metal plates with gradually changing properties buckle under pressure. This method considers how the material properties change throughout the plate's thickness and the influence of the holes within the porous material. Slimani et al. [22] studied how bending affects plates made from materials that gradually change throughout their thickness (functionally graded plates) and contain tiny holes (porosity). The amount of these holes can vary across the plate, creating two main scenarios: either the holes are spread evenly throughout (perfectly homogeneous) or they are concentrated in specific areas (perfect homogeneity shape). Refrafi et al. [23] investigated the vibrations of plates made from materials with gradually changing properties (FG plates) that are supported on all sides (simply supported edges). To achieve this, they employed a sophisticated method that considers the way the plate bends and stretches, along with the variations in material properties throughout its thickness. Messaoudi et al. [24] developed a new approach to analyze the vibrations of plates using a simpler method compared to existing techniques. This method requires solving for fewer unknowns, making it more efficient. Unlike traditional 2D methods, it also considers the effect of the plate stretching in the thickness direction. However, this approach has limitations compared to computer simulations, especially when dealing with complex boundary conditions. Shahsavari et al. [25] presented a study focused on the fourfold coupled (axial–shear–bending–stretching) size-dependent shear buckling force of FG porous nanoplates exposed to hygrothermal environment and lying on Kerr elastic foundation. Bodaghi and Saidi [26] employed the CPT based on exact position of neutral surface to analyze buckling of thin FG plate resting on Pasternak foundation and subjected to non-uniformly distributed in-plane

loading. Singh and Harsha [27] proposed a 2D HSDT solution to investigate the buckling of FG plates exposed to uniform and non-uniformly applied in-plane and transverse load.

Mohammadi et al.[28], study the dynamic behavior of rectangular nanoplates with single-layered graphene sheets laying on an elastic medium subjected to shear in-plane load, based on differential quadrature method. The dynamic behavior of annular and circular graphene sheet surrounding Winkler-Pasternak elastic supports and subjected to thermal and in-plane load, using the nonlocal elasticity theory, have been study by Mohammadi et al. [29]. Mohammadi et al. [30] have studied the effect of the thermal load on the free vibration of mono-layer graphene sheet laying on an elastic foundation. Using the nonlocal elasticity theory to obtain the governing equations and based on Levy and Navier solutions technics, the naturel frequency are obtained for three cases of boundary conditions. Considering the effect of viscosity, the dynamic behavior of nanobeam embedded in the visco-Pasternak foundation subjected to hygro-thermo-mechanical loading have been study by Mohammadi et al. [31]. Chu et al. [32] examine the stability and dynamic response of circular sandwich plates with a special foam core and reinforced faces with graphene platelets in thermal environment. The Chebyshev collocation technic is applied to attain the discrete form of equilibrium and dynamic equations. Based on the novel theory of two-phase local/nonlocal elasticity, wave propagation and vibration of a nano super capacitor based on Kerr viscoelastic foundation including two springs, two dampers, and one shear element are studied by Al-Furjan et al. [33] using refined zigzag theory (RZT). Wan et al. [34] investigate the effects of reinforcing a hybrid nanocomposite viscoelastic rhombic plate with Carbon Nano-Tubes (CNTs) and Carbon Fibers (CFs) laying on a viscoelastic torsional fractional substrate on the post-stability response, naturel and excited vibration . The distribution of CNTs and the structural damping is analyzed using the Halpin-Tsai theory and Kelvin-Voigt method respectively. In addition, the first-order shear deformation theory is used to create the structure model. Al-Furjan et al. [35] study Wave propagation of imperfect functionally graded materials (FGM) and magneto strictive nanocomposite layers. Based on refined zigzag theory (RZT) and the Halpin-Tsai model for the effective material characteristic, the governing equations are gained using Hamilton's principle and solved by exact solutions. Shan et al. [36] exposed a review of the impact of nano-additives in improving the mechanical characteristics and optimization methods in nanocomposite materials. Chu et al. [37] presents the energy absorption, free and forced vibrations of sandwich non-rectangular nanoplates made from alumina reinforced by graphene platelets (GPLs) with a single sinusoidal edge laying on a viscoelastic foundation. Micromechanical Halpin–Tsai distribution and Kelvin–Voigt models are considering to obtain the effective material characteristics and structural damping, correspondingly. Refined zigzag theory (RZT) and Hamilton’s principle are used to derive the coupled electro-magneto-mechanical equations of motion and analyzed by Galerkin’s and Newmark’s procedures. Theoretical evaluation of the impacts of moving load and the use of a piezoelectric patch on the dynamic behavior of a Nano Conical Panel (NCP) laying on viscoelastic foundation via the First-order Shear Deformation Theory (FSDT) has been study by Chu et al. [38]. Boron nitride nanotubes (BNNTs) are used to reinforce the piezoelectric patch. Integral Quadrature (IQ), Differential Quadrature (DQ), and Newmark methods were coupled to solve the equations of motions. Wan et al. [39] examine the nonlinear flutter response and reliability of trapezoidal plates made of hybrid composite core layer reinforced by carbon nanotubes (CNTs) and carbon fibers and subjected to yawed flow using advanced differential Quadrature hierarchical finite element method (DQHFEM). The complexities of the hybrid nanocomposite properties are determined by using the Halpin-Tsai model. Kolahchi et al. [40] optimizes the design of conical shells made from advanced materials for better performance under challenging conditions involving magnets, moisture, and heat. Using Hamilton's principle, the researchers derived the equations governing the motion of the system. These equations were then solved with two techniques: the differential quadrature method and Bolotin's method. This allowed them to determine the range of conditions (dynamic stability region) where the system remains stable.To further improve the system's performance and find the optimal dynamic conditions, the authors proposed a new hybrid optimization method. This method combines particle swarm optimization (PSO) and harmony search algorithms (HS). recently the researcher and his team have several works on static and dynamic behavior solicited on different types of structures [41-50].

Survey of the literature shows that a few studies address the buckling of FG plates subjected to uniform and non-uniformly applied in-plane. In this regard, this paper aims to propose a theoretical formulation based on a quasi-3D solution that includes the stretching effect to study the buckling of FG plate subjected to compressive uniform, linear, and non-linear in-plane loads. Stretching effect plays a very important role in determining the response of thick structures. In addition, several types of foundations will be used such as Winkler, Pasternak and Kerr with various types of boundary conditions. To the best of the authors' knowledge this problem has not been treated before. The proposed model contains undetermined integral terms and involves only four unknown functions. In addition, several boundary conditions will be considered and their effects on the critical buckling load will be determined. The overall material properties of the plates are considered to be varying across the thickness according to a power law. Analytical solution will be used to determine the critical buckling loads. Comparisons studies are carried out in order to validate the efficiency of the present model. Then, parametric studies are conducted allowing

studying and analyzing the effects of power law index, geometry of plate, elastic foundation parameters and boundary conditions on critical buckling load of FG plate resting on elastic foundation.

2. Problem formulation

The geometry and dimensions of the plate resting on elastic foundations are represented in Figure 1. Rectangular Cartesian coordinates (x, y, z) are used to describe infinitesimal deformations FG elastic plate occupying the region $[0,a]\,x\,[0,b]\,x\,[-h/2,\ h/2]$ in the unstressed reference configuration. The top and bottom faces of the plate are at $z=\pm h/2$, and the edges of the plate are parallel to axes x and y. The volume and the area surface are indicated with V and A, respectively.

The effective material properties, like Young's modulus E can be expressed by the rule of mixture as:

$$P\ (z)=P_m+(P_c-P_m)\ V(z) \tag{1}$$

$$V(z)=\left(\frac{z}{h}+\frac{1}{2}\right)^k \tag{2}$$

The subscripts *m* and *c* refer to metal and ceramic. k is the volume fraction index ($0\le k\le+\infty$), which indicates the material variation profile through the thickness.

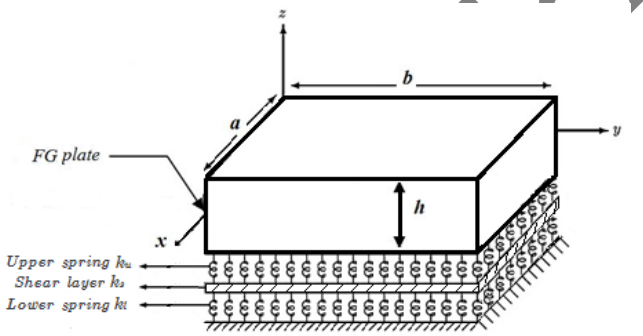

Fig 1: coordinate system and geometry for rectangular FG plates on elastic foundation

The plate is assumed to be subjected to different type of in-plane compressive loading as shown in Fig.2 (Singh and Harsha [27]).

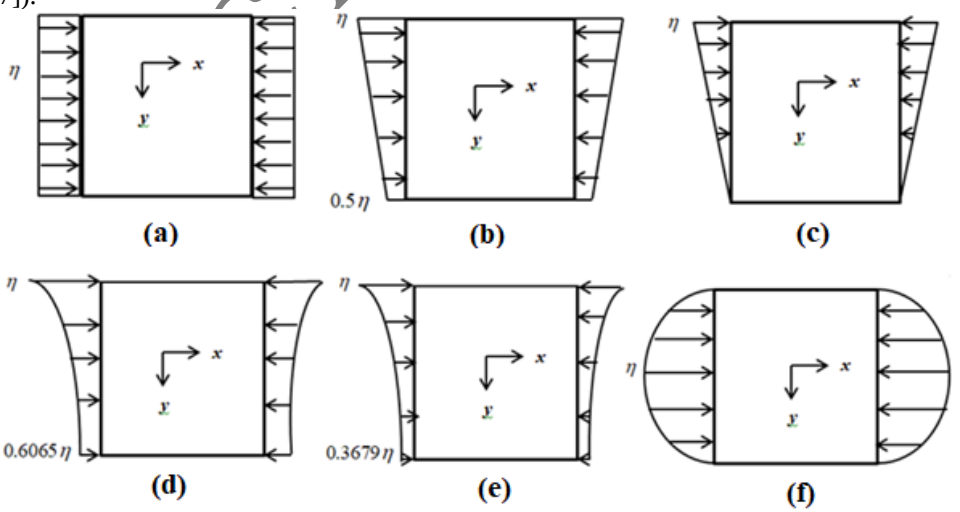

Fig2: schematic representation of different type of in-plane compressive loads (a) uniformly varying load, (b) trapezoidal, (c) triangular, (d-e) exponential varying load, (f) sinusoidal load

2.1. Kinematic

The displacement field satisfying the conditions of transverse shear stresses (and hence strains) vanishing at (x, y, ±h/2) on the outer (top) and inner (bottom) surfaces of the plate, is given as follows [51]:

$$\begin{aligned} u(x,y,z) &= u_0(x,y) - z\frac{\partial w_0}{\partial x} + k_1 f(z)\int \theta dx \\ v(x,y,z) &= v_0(x,y) - z\frac{\partial w_0}{\partial y} + k_2 f(z)\int \theta dy \\ w(x,y,z) &= w_0(x,y) + g(z)\theta(x,y) \end{aligned} \tag{3}$$

Some simplifications are used here to get:

$$\begin{aligned} u(x,y,z) &= u_0(x,y) - z\frac{\partial w_0}{\partial x} + k_1 A f(z)\frac{\partial \theta}{\partial x} \\ v(x,y,z) &= v_0(x,y) - z\frac{\partial w_0}{\partial y} + k_2 B f(z)\frac{\partial \theta}{\partial y} \\ w(x,y,z) &= w_0(x,y) + g(z)\theta(x,y) \end{aligned} \tag{4}$$

And

$$k_1 = \lambda^2, \qquad k_2 = \mu^2, \quad A = -\frac{1}{\lambda^2}, \quad B = -\frac{1}{\mu^2} \tag{5}$$

Where:

$$\lambda = \frac{m\pi}{a}, \qquad \mu = \frac{n\pi}{b} \tag{6}$$

In the present study, the new shape function $f(z)$ is given as follow:

$$f(z) = z\left(\frac{1}{\pi} - \frac{5}{37}\pi\left(\frac{z}{h}\right)^2\right) \tag{7}$$

Where:

$$g(z) = \frac{2}{12}\left(\frac{df(z)}{dz}\right) \tag{8}$$

Based on the small-strain elasticity theory, the linear strain expressions derived from the displacement field are given as follow:

$$\begin{aligned} \varepsilon_{xx} &= \varepsilon_{xx}^0 + z\varepsilon_{xx}^1 + f(z)\varepsilon_{xx}^2 \\ \varepsilon_{yy} &= \varepsilon_{yy}^0 + z\varepsilon_{yy}^1 + f(z)\varepsilon_{yy}^2 \\ \gamma_{xy} &= \gamma_{xy}^0 + z\gamma_{xy}^1 + f(z)\gamma_{xy}^2 \\ \gamma_{yz} &= \frac{\partial f(z)}{\partial z}\gamma_{yz}^0 + g(z)\gamma_{yz}^1 \\ \gamma_{xz} &= \frac{\partial f(z)}{\partial z}\gamma_{xz}^0 + g(z)\gamma_{xz}^1 \\ \varepsilon_{zz} &= g'(z)\varepsilon_{zz}^0 \end{aligned} \tag{9}$$

Where:

$$\left\{\begin{matrix}\varepsilon_{xx}^0\\ \varepsilon_{yy}^0\\ \gamma_{xy}^0\end{matrix}\right\} = \left\{\begin{matrix}\dfrac{\partial u_0}{\partial x}\\ \dfrac{\partial v_0}{\partial y}\\ \dfrac{\partial u_0}{\partial y} + \dfrac{\partial v_0}{\partial x}\end{matrix}\right\}, \quad \left\{\begin{matrix}\varepsilon_{xx}^1\\ \varepsilon_{yy}^1\\ \varepsilon_{xy}^1\end{matrix}\right\} = \left\{\begin{matrix}-\dfrac{\partial^2 w_0}{\partial x^2}\\ -\dfrac{\partial^2 w_0}{\partial y^2}\\ -2\dfrac{\partial^2 w_0}{\partial x \partial y}\end{matrix}\right\} \tag{10}$$

$$\left\{\begin{matrix}\varepsilon_{xx}^{2}\\ \varepsilon_{yy}^{2}\\ \varepsilon_{xy}^{2}\end{matrix}\right\}=\left\{\begin{matrix}k_1A\dfrac{\partial^2\theta}{\partial x^2}\\ k_2B\dfrac{\partial^2\theta}{\partial y^2}\\ (k_1A+k_2B)\dfrac{\partial^2\theta}{\partial x\partial y}\end{matrix}\right\},\quad \left\{\begin{matrix}\gamma_{xz}^{0}\\ \gamma_{yz}^{0}\end{matrix}\right\}=\left\{\begin{matrix}k_1A\dfrac{\partial\theta}{\partial x}\\ k_2B\dfrac{\partial\theta}{\partial y}\end{matrix}\right\},\ \left\{\begin{matrix}\gamma_{xz}^{1}\\ \gamma_{yz}^{1}\end{matrix}\right\}=\left\{\begin{matrix}\dfrac{\partial\theta}{\partial x}\\ \dfrac{\partial\theta}{\partial y}\end{matrix}\right\} \tag{11}$$

The stress–strain relationships for the FG plate are as follows:

$$\left\{\begin{matrix}\sigma_{xx}\\ \sigma_{yy}\\ \sigma_{zz}\\ \tau_{xz}\\ \tau_{yz}\\ \tau_{xy}\end{matrix}\right\}=\begin{bmatrix}C_{11} & C_{12} & C_{13} & 0 & 0 & 0\\ C_{12} & C_{22} & C_{23} & 0 & 0 & 0\\ C_{13} & C_{23} & C_{33} & 0 & 0 & 0\\ 0 & 0 & 0 & C_{44} & 0 & 0\\ 0 & 0 & 0 & 0 & C_{55} & 0\\ 0 & 0 & 0 & 0 & 0 & C_{66}\end{bmatrix}\left\{\begin{matrix}\varepsilon_{xx}\\ \varepsilon_{yy}\\ \varepsilon_{zz}\\ \gamma_{xz}\\ \gamma_{yz}\\ \gamma_{xy}\end{matrix}\right\} \tag{12}$$

The terms C_{ij} are given by:

$$\begin{aligned}C_{11}&=C_{22}=C_{33}=\frac{E\ (z)(1-\nu\ )}{(1-2\nu\ )(1+\nu\ )}\\ C_{12}&=C_{13}=C_{23}=\frac{\nu\ E\ (z)}{(1-2\nu\ )(1+\nu\ )}\\ C_{44}&=C_{55}=C_{66}=\frac{E\ (z)}{2(1+\nu\ )}\end{aligned} \tag{13}$$

2.2. Governing equations

By employing the principle of virtual displacement for which the external work is equal to the internal one, the governing equations of equilibrium for the FG plate are developed as follow:

$$0=\int_V(\delta U+\delta V+\delta U_{\ f}\ )dV \tag{14}$$

Where δU is the variation of strain energy, δV is the variation of the external work done by external load applied to the plate and δU_f is the variation of strain energy of foundation

$$\delta U=\int_V\left[\sigma_{xx}\,\delta\varepsilon_{xx}+\sigma_{yy}\,\delta\varepsilon_{yy}+\sigma_{zz}\,\delta\varepsilon_{zz}+\tau_{xy}\,\delta\gamma_{xy}+\tau_{yz}\,\delta\gamma_{yz}+\tau_{xz}\,\delta\gamma_{xz}\right]dV \tag{15}$$

$$\delta U=\int_\Omega\left[\begin{matrix}N_{xx}\,\delta\varepsilon_{xx}^{0}+M_{xx}\,\delta\varepsilon_{xx}^{1}+P_{xx}\,\delta\varepsilon_{xx}^{2}+N_{yy}\,\delta\varepsilon_{yy}^{0}+M_{yy}\,\delta\varepsilon_{yy}^{1}+P_{yy}\,\delta\varepsilon_{yy}^{2}\\ +N_{zz}\,\delta\varepsilon_{zz}^{0}+N_{xy}\,\delta\varepsilon_{xy}^{0}+M_{xy}\,\delta\varepsilon_{xy}^{1}+P_{xy}\,\delta\varepsilon_{xy}^{2}+Q_{yz}\delta\gamma_{yz}^{0}+Q_{xz}\,\delta\gamma_{xz}^{0}\\ +S_{yz}\delta\gamma_{yz}^{1}+S_{xz}\,\delta\gamma_{xz}^{1}\end{matrix}\right]dA \tag{16}$$

The stress, moment and additional moment resultants ***N, M, P*** and ***Q*** of the FG plate are expressed by:

$$\left\{\begin{matrix}N_{xx}\\ N_{yy}\\ N_{xy}\end{matrix}\right\}=\int_{-h/2}^{h/2}\left\{\begin{matrix}\sigma_{xx}\\ \sigma_{yy}\\ \tau_{xy}\end{matrix}\right\}z\,d\,z,\quad \left\{\begin{matrix}M_{xx}\\ M_{yy}\\ M_{xy}\end{matrix}\right\}=\int_{-h/2}^{h/2}\left\{\begin{matrix}\sigma_{xx}\\ \sigma_{yy}\\ \tau_{xy}\end{matrix}\right\}z\,d\,z \tag{17}$$

$$\left\{\begin{matrix}P_{xx}\\ P_{yy}\\ P_{xy}\end{matrix}\right\}=\int_{-h/2}^{h/2}\left\{\begin{matrix}\sigma_{xx}\\ \sigma_{yy}\\ \tau_{xy}\end{matrix}\right\}f(z)\,d\,z,\quad \left\{\begin{matrix}Q_{xz}\\ Q_{yz}\end{matrix}\right\}=\int_{-h/2}^{h/2}\left\{\begin{matrix}\tau_{xz}\\ \tau_{yz}\end{matrix}\right\}^{(n)}g(z)\,d\,z \tag{18}$$

$$\left\{\begin{matrix}S_{xz}\\ S_{yz}\end{matrix}\right\}=\int_{-h/2}^{h/2}\left\{\begin{matrix}\tau_{xz}\\ \tau_{yz}\end{matrix}\right\}^{(n)}\frac{\partial f(z)}{\partial z}d\,z,\quad \{N_{zz}\}=\int_{-h/2}^{h/2}\{\sigma_{zz}\}^{(n)}\,g'(z)d\,z, \tag{19}$$

Substituting Eq. (5) into Eq. (7) and the subsequent results into Eq. (12), the stress resultants of the FG plate can be related to the total strains by:

$$\begin{Bmatrix} N_{xx} \\ N_{yy} \\ N_{xy} \\ M_{xx} \\ M_{yy} \\ M_{xy} \\ P_{xx} \\ P_{yy} \\ P_{xy} \\ N_{zz} \end{Bmatrix} = \begin{bmatrix} A_{11} & A_{12} & 0 & B_{11} & B_{12} & 0 & Cs_{11} & Cs_{12} & 0 & X_{13} \\ A_{12} & A_{22} & 0 & B_{12} & B_{22} & 0 & Cs_{12} & Cs_{22} & 0 & X_{23} \\ 0 & 0 & A_{66} & 0 & 0 & B_{66} & 0 & 0 & Cs_{66} & 0 \\ B_{11} & B_{12} & 0 & D_{11} & D_{12} & 0 & F_{11} & F_{12} & 0 & Y_{13} \\ B_{12} & B_{22} & 0 & D_{12} & D_{22} & 0 & F_{12} & F_{22} & 0 & Y_{23} \\ 0 & 0 & B_{66} & 0 & 0 & D_{66} & 0 & 0 & F_{66} & 0 \\ Cs_{11} & Cs_{12} & 0 & F_{11} & F_{12} & 0 & H_{11} & H_{12} & 0 & R_{13} \\ Cs_{12} & Cs_{22} & 0 & F_{12} & F_{22} & 0 & H_{12} & H_{22} & 0 & R_{23} \\ 0 & 0 & Cs_{66} & 0 & 0 & F_{66} & 0 & 0 & H_{66} & 0 \\ X_{13} & X_{23} & 0 & Y_{13} & Y_{23} & 0 & R_{13} & R_{23} & 0 & Z_{33} \end{bmatrix} \begin{Bmatrix} \varepsilon_{xx}^0 \\ \varepsilon_{yy}^0 \\ \varepsilon_{xy}^0 \\ \varepsilon_{xx}^1 \\ \varepsilon_{yy}^1 \\ \varepsilon_{xy}^1 \\ \varepsilon_{xx}^2 \\ \varepsilon_{yy}^2 \\ \varepsilon_{xy}^2 \\ \varepsilon_{zz}^0 \end{Bmatrix} \tag{20}$$

$$\begin{Bmatrix} S_{xz} \\ S_{yz} \\ Q_{xz} \\ Q_{yz} \end{Bmatrix} = \begin{bmatrix} G_{44}^0 & G_{44}^1 & 0 & 0 \\ 0 & 0 & G_{55}^0 & G_{55}^1 \\ G_{44}^1 & G_{66} & 0 & 0 \\ 0 & 0 & G_{55}^1 & G_{66} \end{bmatrix} \begin{Bmatrix} \gamma_{xz}^0 \\ \gamma_{yz}^1 \\ \gamma_{yz}^0 \\ \gamma_{yz}^1 \end{Bmatrix}, \tag{21}$$

Where: A_{ij}, B_{ij}, Cs_{ij} …etc. are the plate stiffness's, defined as follow:

$$\begin{Bmatrix} A_{11} & B_{11} & D_{11} & Cs_{11} & F_{11} & H_{11} \\ A_{12} & B_{12} & D_{12} & Cs_{12} & F_{12} & H_{12} \\ A_{66} & B_{66} & D_{66} & Cs_{66} & F_{66} & H_{66} \end{Bmatrix} = \int_{-h/2}^{h/2} [1, z, z^2, f(z), z\,f(z), f^2(z)] \begin{Bmatrix} C_{11} \\ C_{12} \\ C_{66} \end{Bmatrix} dz \tag{22}$$

$$\left(A_{22}, B_{22}, D_{22}, C_{22}, F_{22}, H_{22}\right) = \left(A_{11}, B_{11}, D_{11}, C_{11}, F_{11}, H_{11}\right) \tag{23}$$

$$\begin{aligned} G_{44}^0 &= G_{55}^0 = \int_{-h/2}^{h/2} C_{44} \left[\frac{\partial f(z)}{\partial z}\right]^2 dz \\ G_{44}^1 &= G_{55}^1 = \int_{-h/2}^{h/2} C_{44} \left[\frac{\partial f(z)}{\partial z}\right] g(z) dz \\ G_{66} &= \int_{-h/2}^{h/2} C_{66} \left[g(z)\right]^2 dz \end{aligned} \tag{24}$$

$$\left\{X_{ij}, Y_{ij}, R_{ij}, Z_{ii}\right\} = \sum_{n=1}^{3} \int_{h_{n-1}}^{h_n} C_{ij} \left\{1, z, f(z), g'(z)\right\} g'(z) d\,z \tag{25}$$

The variation of work done by in-plane loads is given by:

$$\delta V = -\int_A \bar{N} \delta w \, dA = -\int_A \bar{N} (\delta w_0 + g(z) \delta\theta) \, dA \tag{26}$$

With:

$$\bar{N} = \left[N_x^0 \frac{\partial^2 w}{\partial x^2} + N_{xy}^0 \frac{\partial^2 w}{\partial x \partial y} N_y^0 \frac{\partial^2 w}{\partial y^2} \right] \tag{27}$$

The variation of strain energy of foundation is expressed as:

$$\delta U_f = \int_A f_e \delta w \, dA = \int_A f_e (\delta w_0 + g(z) \delta\theta) \, dA \tag{28}$$

Where $\mathbf{f_e}$ is the density of reaction force of foundation. For the Pasternak foundation model:

$$\begin{aligned} f_e &= \bar{K} w - \bar{G} \nabla^2 w \\ \bar{K} &= k_w, \; \bar{G} = k_g \end{aligned} \tag{29}$$

The Kerr model foundation is a three-parameter elastic model that consists of a shear layer (with stiffness) independent upper (with stiffness) and lower (with stiffness) elastic layers (modeled by distributed springs). The distributed reaction of Kerr foundation model is defined as:

$$f_e = \bar{K}w - \bar{G}\nabla^2 w$$
$$\bar{K} = \frac{k_l k_u}{k_l + k_u},\ \bar{G} = \frac{k_s k_u}{k_l + k_u} \tag{30}$$

Substituting equations (10) and (11) into the equation (16), given equation is combined with equations (26) and (28), the governing equations of stability can be expressed as follows:

$$\delta u_0 : \quad \frac{\partial N_{xx}}{\partial x} + \frac{\partial N_{xy}}{\partial y} = 0$$
$$\delta v_0 : \quad \frac{\partial N_{xy}}{\partial x} + \frac{\partial N_{yy}}{\partial y} = 0$$
$$\delta w_0 : \quad \frac{\partial^2 M_{xx}}{\partial x^2} + 2\frac{\partial^2 M_{xy}}{\partial x \partial y} + \frac{\partial^2 M_{yy}}{\partial y^2} + \bar{N} + f_e = 0 \tag{31}$$
$$\delta\theta : \quad -K_1 A\frac{\partial^2 P_{xx}}{\partial x^2} - K_2 B\frac{\partial^2 P_{yy}}{\partial y^2} - (K_1 A + K_2 B)\frac{\partial^2 P_{xy}}{\partial x \partial y} +$$
$$K_1 A\frac{\partial S_{xz}}{\partial x} + K_2 B\frac{\partial S_{yz}}{\partial y} + \frac{\partial Q_{xz}}{\partial x} + \frac{\partial Q_{yz}}{\partial y} - N_{zz} + g(z)\bar{N} + g(z) f_e = 0$$

Substituting equations (10), (11), (20) and (21) into equation (31), the governing equations of stability of the FG plate are defined by:

$$\delta u_0 : \quad A_{11}\frac{\partial^2 u_0}{\partial x^2} + A_{66}\frac{\partial^2 u_0}{\partial y^2} + (A_{12} + A_{66})\frac{\partial^2 v_0}{\partial x \partial y} - B_{11}\frac{\partial^3 w_0}{\partial x^3} - (B_{12} + 2B_{66})\frac{\partial^3 w_0}{\partial x \partial y^2}$$
$$+ Cs_{11} K_1 A\frac{\partial^3 \theta}{\partial x^3} + (Cs_{12} K_2 B + Cs_{66}(K_1 A + K_2 B))\frac{\partial^3 \theta}{\partial x \partial y^2} + X_{13}\frac{\partial \theta}{\partial x} = 0 \tag{32a}$$

$$\delta v_0 : \quad (A_{12} + A_{66})\frac{\partial^2 u_0}{\partial x \partial y} + A_{22}\frac{\partial^2 v_0}{\partial y^2} + A_{66}\frac{\partial^2 v_0}{\partial x^2} - B_{22}\frac{\partial^3 w_0}{\partial y^3} - (B_{12} + 2B_{66})\frac{\partial^3 w_0}{\partial x^2 \partial y}$$
$$+ Cs_{22} K_2 B\frac{\partial^3 \theta}{\partial y^3} + (Cs_{12} K_1 A + Cs_{66}(K_1 A + K_2 B))\frac{\partial^3 \theta}{\partial x^2 \partial y} + X_{23}\frac{\partial \theta}{\partial y} = 0 \tag{32b}$$

$$\delta w_0 : \quad B_{11}\frac{\partial^3 u_0}{\partial x^3} + (B_{12} + 2B_{66})\frac{\partial^3 u_0}{\partial x \partial y^2} + B_{22}\frac{\partial^3 v_0}{\partial y^3} + (B_{12} + 2B_{66})\frac{\partial^3 v_0}{\partial x^2 \partial y}$$
$$- D_{11}\frac{\partial^4 w_0}{\partial x^4} - D_{22}\frac{\partial^4 w_0}{\partial y^4} - 2(D_{12} + 2D_{66})\frac{\partial^4 w_0}{\partial x^2 \partial y^2} + F_{11} K_1 A\frac{\partial^4 \theta}{\partial x^4} + F_{22} K_2 B\frac{\partial^4 \theta}{\partial y^4}$$
$$+ (F_{12} + 2F_{66})(K_1 A + K_2 B)\frac{\partial^4 \theta}{\partial x^2 \partial y^2} + Y_{13}\frac{\partial^2 \theta}{\partial x^2} + Y_{23}\frac{\partial^2 \theta}{\partial y^2}) N_x^0\frac{\partial^2 w_0}{\partial x^2} + N_{xy}^0\frac{\partial^2 w_0}{\partial x \partial y} \tag{32c}$$
$$+ N_y^0\frac{\partial^2 w_0}{\partial y^2} + \bar{K}w_0 - \bar{G}(\frac{\partial^2 w_0}{\partial x^2} + \frac{\partial^2 w_0}{\partial y^2}) = 0$$

$$\delta\theta : \quad - Cs_{11} K_1 A\frac{\partial^3 u_0}{\partial x^3} - (Cs_{12}\ K_2 B + Cs_{66}(K_1 A + K_2 B)\frac{\partial^3 u_0}{\partial x \partial y^2} - X_{13}\frac{\partial u_0}{\partial x} - Cs_{22} K_2 B\frac{\partial^3 v_0}{\partial x^3}$$
$$- (Cs_{12} K_1 A + Cs_{66}(K_1 A + K_2 B))\frac{\partial^3 v_0}{\partial x^2 \partial y} - X_{23}\frac{\partial v_0}{\partial y} + F_{11} K_1 A\frac{\partial^4 w_0}{\partial x^4} + F_{22}\ K_2 B\frac{\partial^4 w_0}{\partial y^4}$$
$$+ (K_1 A + K_2 B)(F_{12} + 2F_{66})\frac{\partial^4 w_0}{\partial x^2 \partial y^2} + Y_{13}\ \frac{\partial^2 w_0}{\partial x^2} + Y_{23}\ \frac{\partial^2 w_0}{\partial y^2} - H_{11}(K_1 A)^2\frac{\partial^4 \theta}{\partial x^4} -$$
$$H_{22}(K_2 B)^2\frac{\partial^4 \theta}{\partial y^4} - (2H_{12}(K_1 A)(K_2 B) + H_{66}(K_1 A + K_2 B)^2)\frac{\partial^4 \theta}{\partial x^2 \partial x^2} + ((K_1 A)^2 G_{44}^0 +$$
$$2K_1 A\ G_{44}^1 + G_{66} - 2R_{13}(K_1 A))\frac{\partial^2 \theta}{\partial x^2} + ((K_2 B)^2 G_{55}^0 + 2K_2 B\ G66 + G_{66} - 2R_{23}(K_2 B))\frac{\partial^2 \theta}{\partial y^2} - \tag{32d}$$
$$Z_{33} - g(z)\left(N_x^0\frac{\partial^2 w}{\partial x^2} - N_{xy}^0\frac{\partial^2 w}{\partial x \partial y} - N_y^0\frac{\partial^2 w}{\partial y^2}\right) + g(z)\left(\bar{K}w_0 - \bar{G}(\frac{\partial^2 w_0}{\partial x^2} + \frac{\partial^2 w_0}{\partial y^2})\right) = 0$$

2.3. Solution for FG plate with various boundary conditions

Solution of Eq. (32) for the FGMs plate under various boundary conditions can be constructed. To solve the governing equations based on the proposed theory, a general solution of different boundary conditions is used. To this end, the displacement field can be assumed as

$$\begin{Bmatrix} u_0(x,y) \\ v_0(x,y) \\ w_0(x,y) \\ \theta(x,y) \end{Bmatrix} = \begin{Bmatrix} U_{mn} & \dfrac{\partial X_m(x)}{\partial x} Y_n(y) \\ V_{mn} & X_m(x) \dfrac{\partial Y_n(y)}{\partial y} \\ W_{mn} & X_m(x) Y_n(y) \\ \phi_{mn} & X_m(x) Y_n(y) \end{Bmatrix} \tag{33}$$

Where U ,V ,W and ψ are arbitrary parameters to be determined. The functions $X_m(x)$ and $Y_n(y)$ are suggested here to satisfy the geometric boundary conditions and represent approximate shapes of the deflected surface of the plate. These functions, for the different cases of boundary conditions, are listed in Table 1.

Substituting equations (33) into equations (32), the obtained equations are expressed as follow:

$$[M]\{\Delta\} = \{0\} \tag{34}$$

Where $\{\Delta\}$ denotes the transposed columns

$$\{\Delta\} = \{U_{mn}, V_{mn}, W_{mn}, \phi_{mn}\}^T \tag{35}$$

$[K]$ is the symmetric matrix given by:

$$[K] = \begin{bmatrix} M_{11} & M_{12} & M_{13} & M_{14} \\ M_{21} & M_{22} & M_{23} & M_{24} \\ M_{31} & M_{32} & M_{33} + \zeta(y) & M_{34} + g(z)\zeta(y) \\ M_{41} & M_{42} & M_{43} + g(z)\zeta(y) & M_{44} + (g(z))^2 \zeta(y) \end{bmatrix} \tag{36}$$

The elements M_{ij} are expressed as follow:

$$\begin{aligned}
M_{11} &= A_{11}\alpha_{12} + A_{66}\alpha_8 \\
M_{12} &= (A_{12} + A_{66})\alpha_8 \\
M_{13} &= -B_{11}\alpha_{12} - (B_{12} + 2B_{66})\alpha_8 \\
M_{14} &= (Cs_{12}K_2B + Cs_{66}(K_1A + K_2B))\alpha_8 + Cs_{11}K_1A\,\alpha_{12} + X_{13}\alpha_6 \\
M_{21} &= (A_{12} + A_{66})\alpha_{10} \\
M_{22} &= A_{22}\alpha_4 + A_{66}\alpha_{10} \\
M_{23} &= -B_{11}\alpha_4 - (B_{12} + 2B_{66})\alpha_{10} \\
M_{24} &= -Cs_{22}K_2B\,\alpha_4 - (Cs_{12}K_1A \\
&\quad + Cs_{66}(K_1A + K_2B))\alpha_{10} + X_{13}\alpha_2 \\
M_{31} &= B_{11}\alpha_{13} + (B_{12} + 2B_{66})\alpha_{11} \\
M_{32} &= B_{11}\alpha_5 + (B_{12} + 2B_{66})\alpha_{11} \\
M_{33} &= -D_{11}\alpha_{13} - D_{22}\alpha_5 - 2(D_{12} + 2D_{66})\alpha_{11} + \bar{K} - \bar{G}(\lambda^2 + \mu^2) \\
M_{34} &= F_{11}K_1A\alpha_{13} + (F_{12} + 2F_{66})(K_1A + K_2B))\alpha_{11} + F_{22}K_2B\alpha_5 \\
&\quad + Y_{13}\alpha_9 + Y_{23}\alpha_3 + g(z)\bar{K} + g(z)\bar{G}(\lambda^2 + \mu^2) \\
M_{41} &= -(Cs_{12}K_2B + Cs_{66}(K_1A + K_2B))\,\alpha_{11} - Cs_{11}K_1A\,\alpha_{13} - X_{13}\,\alpha_9 \\
M_{42} &= -Cs_{22}K_2\,\alpha_5 - (Cs_{12}K_1A + Cs_{66}(K_1A + K_2B))\alpha_{11} - X_{23}\,\alpha_3 \\
M_{43} &= F_{11}K_1A\alpha_{13} + (F_{12} + 2F_{66})(K_1A + K_2B))\alpha_{11} + F_{22}K_2B\alpha_5 \\
&\quad + Y_{13}\,\alpha_9 + Y_{23}\,\alpha_3 + g(z)\bar{K} + g(z)\bar{G}(\lambda^2 + \mu^2) \\
M_{44} &= -(K_1A)^2 H_{11}\alpha_{13} - H_{22}(K_2B)^2\alpha_5 - (2H_{12}K_1AK_2B \\
&\quad + H_{66}(K_1A + K_2B)^2)\alpha_{11} + (G^0_{44}(K_1A)^2 + 2G^1_{44}(K_1A) \\
&\quad + G_{66} - 2R_{13}(K_1A))\alpha_9 + (G^0_{44}(K_2B)^2 + 2G^1_{44}(K_2B) \\
&\quad + G_{66} - 2R_{23}(K_2B))\alpha_3 - Z_{33}\alpha_1 + g(z)^2\bar{K} + g(z)^2\bar{G}(\lambda^2 + \mu^2)
\end{aligned} \tag{37}$$

With $\zeta(y) = -N_0(\alpha_9 + \eta\alpha_3),\ N_x^0 = -N_0,\ \ N_y^0 = -\chi\eta N_0,\ \ \frac{N_x^0}{N_y^0} = \eta,\ N_{xy}^0 = 0$ (38)

And

$$(\alpha_1, \alpha_2, \alpha_3, \alpha_4) = \int_0^a\int_0^b \left(X_m'''Y_n, X_m'Y_n'', X_m'Y_n, X_m'Y_n''\right)X_m'Y_n\, dxdy \ ,(\alpha_5, \alpha_6, \alpha_7) = \int_0^a\int_0^b \left(X_m''Y_n', X_mY_n''', X_mY_n'\right)X_mY_n'\, dxdy$$

$$(\alpha_8, \alpha_9, \alpha_{10}) = \int_0^a\int_0^b \left(X_m'''Y_n, X_m''Y_n'', X_m''Y_n\right)X_mY_n\, dxdy \ ,(\alpha_{11}, \alpha_{12}, \alpha_{13}) = \int_0^a\int_0^b \left(X_mY_n''', X_mY_n'', X_mY_n\right)X_mY_n\, dxdy \quad (39)$$

The used non-dimensional parameters are

$$\hat{N} = \frac{N_{cr}.b^2}{D_0} = \frac{12(1-\nu^2)N_{cr}.b^2}{E_c.h^3}, k_w = \frac{K_wa^2}{D},$$
$$k_p = \frac{K_pa^2}{D}, k_u = \frac{K_ua^2}{D}, k_s = \frac{K_sa^2}{D}, k_l = \frac{K_la^2}{D}, D = \frac{h^3E_c}{12(1-\nu^2)} \quad (40)$$

Table 1: The admissible functions Xm(x) and Yn(y) [52, 53]

	Boundary conditions		The functions X_m and Y_n	
	at$x$= *0,a*	at$y$= *0,b*	$X_m(x)$	$Y_n(y)$
SSSS	$X_m(0) = X_m''(0) = 0$	$Y_n(0) = Y_n''(0) = 0$	$\sin(\lambda x)$	$\sin(\mu y)$
	$X_m(a) = X_m''(a) = 0$	$Y_n(b) = Y_n''(b) = 0$		
CSSS	$X_m(0) = X_m'(0) = 0$	$Y_n(0) = Y_n''(0) = 0$	$\sin(\lambda x)\left[\cos(\lambda x) - 1\right]$	$\sin(\mu y)$
	$X_m(a) = X_m''(a) = 0$	$Y_n(b) = Y_n''(b) = 0$		
CSCS	$X_m(0) = X_m'(0) = 0$	$Y_n(0) = Y_n'(0) = 0$	$\sin(\lambda x)\left[\cos(\lambda x) - 1\right]$	$\sin(\mu y)\left[\cos(\mu y) - 1\right]$
	$X_m(a) = X_m''(a) = 0$	$Y_n(b) = Y_n'(b) = 0$		
CCSS	$X_m(0) = X_m'(0) = 0$	$Y_n(b) = Y_n''(b) = 0$	$\sin^2(\lambda x)$	$\sin(\mu y)$
	$X_m(a) = X_m'(a) = 0$	$Y_n(b) = Y_n''(b) = 0$		
CCCC	$X_m(0) = X_m'(0) = 0$	$Y_n(0) = Y_n'(0) = 0$	$\sin^2(\lambda x)$	$\sin^2(\mu y)$
	$X_m(a) = X_m'(a) = 0$	$Y_n(b) = Y_n'(b) = 0$		
FFCC	$X_m''(0) = X_m'''(0) = 0$	$Y_n(0) = Y_n'(0) = 0$	$\cos^2(\lambda x)\left[\sin^2(\lambda x) + 1\right]$	$\sin^2(\mu y)$
	$X_m''(a) = X_m'''(a) = 0$	$Y_n(b) = Y_n'(b) = 0$		
FFSS	$X_m''(0) = X_m'''(0) = 0$	$Y_n(b) = Y_n''(b) = 0$	$\cos^2(\lambda x)\left[\sin^2(\lambda x) + 1\right]$	$\sin(\mu y)$
	$X_m''(a) = X_m'''(a) = 0$	$Y_n(b) = Y_n''(b) = 0$		

( )' Denotes the derivative with respect to the corresponding coordinates.

3. Expression of in-plane load [27]

The in-plane compressive load applied is of the form:

$$N_x^0 = -\eta\zeta(y), N_y^0 = -\chi\eta\zeta(y), N_{xy}^0 = 0 \quad (41)$$

where η is the magnitude of the in-plane buckling load applied in the x-direction.

$\zeta(y)$ is defined as a function representing the variation of in-plane load along the y-axis (see table 2). χ is the non-dimensional load parameter. It takes two values, $\chi = 0$ for uniaxial compression and $\chi = 1$ for biaxial compression.

Ω_0 is a parameter which controls the shape of a function defining in-plane load

$$\lambda(\Omega_0) = \frac{1}{w}\int_0^b \zeta(y)\sin\left(\frac{r\pi y}{b}\right)\sin\left(\frac{j\pi y}{b}\right)dy \quad (42)$$

w is a constant parameter determined during post-processing and gives satisfactory results for one parameter approximation only, $r = j = 1$, and is equal to $b/2$.

$\Omega_0 = 0$ for uniform distributed compressive load, $\Omega_0 = 1$, for compressive triangular load and $0 \prec \Omega_0 \prec 1$ for trapezoidal compressive load.

Table 2: Different type of variations in-plane load [27]

	Load behavior	$\zeta(y)$	$\lambda(\Omega_0)$
1	Uniformly varying (UVL)	$1-\frac{\Omega_0 y}{b}$	$1-\frac{\Omega_0}{2}$
2	Sinusoidal (SL)	$\sin\left(\frac{\pi y}{b}\right)$	$\frac{8}{3\pi}$
3	Exponential (EL)	$e^{\frac{\Omega_0 y}{b}}$	$\frac{4\pi^2 e^{\Omega_0}\left(e^{\Omega_0}-1\right)}{\Omega_0\left({\Omega_0}^2+4\pi^2\right)}$

4. Numerical results and discussion

In this section, various examples are introduced for the buckling of FG plate resting on Kerr/Pasternak/Winkler foundation with general boundary condition. The composed plate is made of Aluminuim (Al) and Alumina (Al2O3) with the following properties:

- ✓ Alumina, Al_2O_3: $E = 380\times10^9$ N/m^2;
- ✓ Aluminium, Al: $E = 70\times10^9$ N/m^2;

The Poisson's ratio is assumed as constant for all results $(\upsilon = 0,3)$.

In order to verify the accuracy of the present formulations, the non-dimensionalized buckling load $\hat{N}$ of FG plate simply supported and without elastic foundation predicted using the quasi-3D solution is compared with the 2D solution of Singh and Harsha [27] as listed in Tables 3-5. The results are presented for different values of power law exponent "*k*", shape parameter "Ω_0" and for three compressive in-plane load (UVL, EL and SL). Note that, in these tables, the span-to-thickness ratio (*a/h*) is taken to be equal to 10.

Table 3. Comparison of non-dimensional critical buckling loads $\hat{N}$ (UVL = Uniformly Varying Load)

b/a	Ω_0	*k=1*		*k=4*		*k=10*	
		Ref [27]	Present	Ref [27]	Present	Ref [27]	Present
1	**0**	9.3391	9.57315	6.23988	6.50800	5.45286	5.59653
	0.25	10.6733	10.9407	7.13129	7.43773	6.23184	6.39603
	0.5	12.4521	12.7642	8.31984	8.67734	7.27048	7.46204
	0.75	14.9426	15.3170	9.98381	10.4128	8.72458	8.95444
	1	18.6782	19.1463	12.4798	13.0160	10.9057	11.1931
2	**0**	3.75015	3.81066	2.53616	2.60333	2.20779	2.24664
	0.25	4.28588	4.35503	2.89847	2.97523	2.52318	2.56760
	0.5	5.0002	5.08087	3.38155	3.47110	2.94371	2.99553
	0.75	6.00024	6.09704	4.05786	4.16531	3.53246	3.59464
	1	7.5003	7.62131	5.07232	5.20664	4.41557	4.49330
5	**0**	2.59144	2.65196	1.74857	1.81420	1.53236	1.56720
	0.25	2.96165	3.03081	1.99836	2.07337	1.75126	1.79109
	0.5	3.45526	3.53594	2.33142	2.41893	2.04314	2.08960
	0.75	4.14631	4.24313	2.79771	2.90271	2.45177	2.50751
	1	5.18289	5.30391	3.49714	3.62840	3.06471	3.13440

Table 4. Comparison of non-dimensional critical buckling loads $\hat{N}$ (EL = Exponential Load).

b/a	Ω_0	*k=1*		*k=4*		*k=10*	
		Ref [27]	Present	Ref [27]	Present	Ref [27]	Present
1	**0**	9.3391	9.57315	6.23988	6.50800	5.45286	5.59653
	0.25	10.5718	10.8367	7.13129	7.36701	6.23184	6.33523
	0.5	11.9428	12.2421	8.31984	8.32240	7.27048	7.15681
	0.75	13.4641	13.8016	9.98381	9.38255	8.72458	8.06848
	1	15.1485	15.5281	12.4798	10.5563	10.9057	9.07784
2	**0**	3.75015	3.81066	2.53616	2.60333	2.20779	2.24664
	0.25	4.24514	4.31363	2.89847	2.94694	2.52318	2.54318
	0.5	4.79567	4.87304	3.38155	3.32911	2.94371	2.87300
	0.75	5.40657	5.49380	4.05786	3.75320	3.53246	3.23898
	1	6.08292	6.18107	5.07232	4.22271	4.41557	3.64417
5	**0**	2.59144	2.65196	1.74857	1.81420	1.53236	1.56720
	0.25	2.93349	3.00200	1.99836	2.05366	1.75126	1.77406
	0.5	3.31392	3.39131	2.33142	2.31999	2.04314	2.00413
	0.75	3.73607	3.82331	2.79771	2.61551	2.45177	2.25943
	1	4.20345	4.30160	3.49714	2.94271	3.06471	2.54207

Table 5. Comparison of non-dimensional critical buckling loads (SL = Sinusoidal Load)

b/a	Ω_0	*k=1*		*k=4*		*k=10*	
		Ref [27]	Present	Ref [27]	Present	Ref [27]	Present
1	**0**	11.002	11.2781	7.3511	7.66707	6.424	6.59326
2	**0**	4.4180	4.48933	2.9878	3.06697	2.6009	2.64677
5	**0**	3.0529	3.12426	2.0599	2.13730	1.8052	1.84631

As can be seen from these tables, a good agreement is observed between the results of the present quasi 3D solution and those of the 2D solution of Singh and Harsha [27]. However, a slight deviation is noticed between the results. This can be justified by the fact that the results reported in the tables are for a value of a/h=10 which corresponds to the case of a thick plate.

For this case, the stretching effect plays an important role in determining the response of the plate. The latter is neglected in formulation of Singh and Harsha [27] since it is a 2D theory and is taken into account in the present formulation.

In addition, the following information can be derived from these tables:

- ✓ For Uniformly varying load (UVL), the critical buckling load almost doubles in value from uniform $(\Omega_0 = 0)$ to triangular loading $(\Omega_0 = 1)$. For Exponential Load (EL), this increase is more than 60%.

- ✓ Increasing the geometry ratio (b/a) leads to a reduction in the critical buckling load, irrespective of the type of loading and the value of the "k" index.

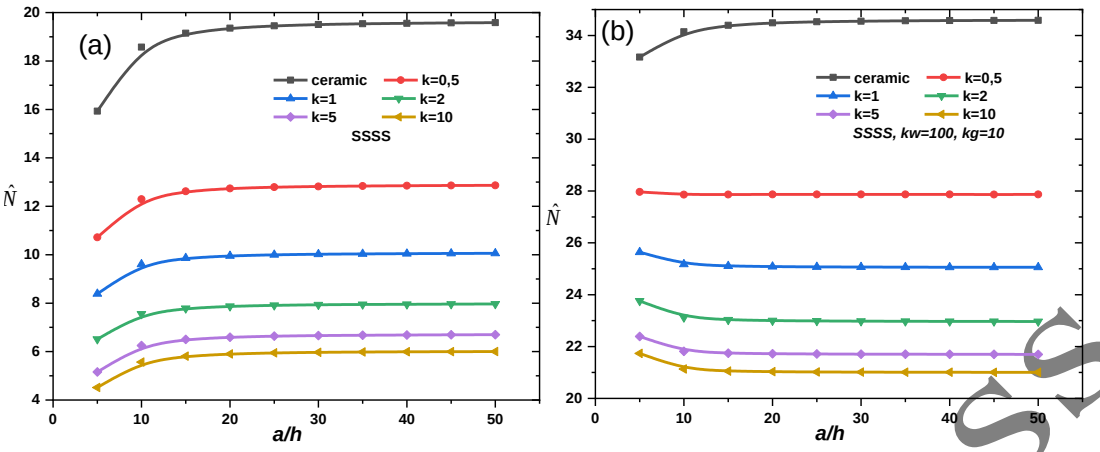

Fig 3. Variation of the critical buckling load ($\hat{N}$) versus the side-to-thickness ratio "a/h" for a simply supported FG plate. (a) plate without elastic foundation , (b) plate on Pasternak elastic foundation (UVL, a/b=1, $\Omega_0 = 0$)

In figure 3, the variation of the critical buckling load as a function of the *a/h* ratio is plotted for different plate configurations (variation of the volume fraction index *k*). The plate is considered simply supported and subjected to UVL with and without an elastic foundation. For the two cases treated, the highest critical loads are obtained for an isotropic ceramic plate.

Also, it is found that with the increase in values of volume fraction index, the volume fraction of metal content in FG plate increases which leads to a reduction in stiffness and consequently, the critical buckling load decreases. The comparison between the two figures (a) and (b) reveals that the incorporation of an elastic foundation increases the critical buckling loads of the plate regardless of its composition. This is due to the increase in plate stiffness generated by the elastic foundation. It can also be seen that the ratio *a/h* affects the critical buckling load only in the thick plate area $(a/h \approx 10)$. Exceeding this area, its influence is minimal.

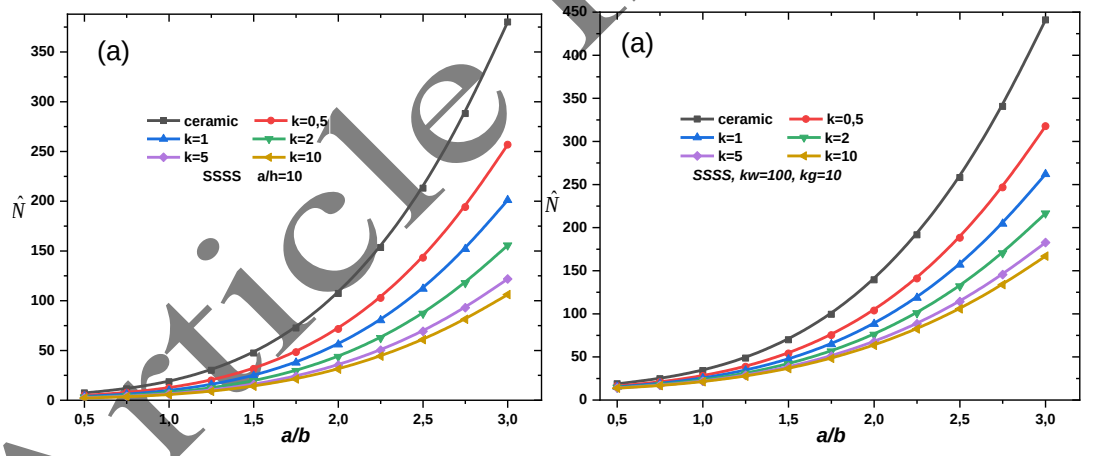

Fig 4. Variation of the critical buckling load ($\hat{N}$) versus the aspect ratio "a/b" for a simply supported FG plate. (a) Plate without elastic foundation, (b) plate on Pasternak elastic foundation (UVL, $\Omega_0 = 0$)

The variation of the critical load $\hat{N}$ as a function of the geometric ratio (*a/b*) is shown in figure 4 for two cases with and without foundation. Several types of plaques are analyzed. It is found that the critical buckling load increases with increasing (*a/b*) ratio and that the highest critical buckling loads are obtained for an isotropic ceramic plate.

The effect of the elastic foundation parameters on the critical buckling load is shown in Figure 5 (a-b). For both figures, the increase in either parameter leads to an increase in the critical buckling load. This can be explained by the fact that the increase in the parameters of the elastic foundation leads to an increase in the rigidity of the plate and consequently the increase in the critical buckling loads. In addition, the increase in the Pasternak parameter generates an increase in the critical load compared to that of Winkler.

Also, the *a/h* ratio, and as mentioned above, affects the critical load only for the case of thick plates (as is the case for *a/h* = 5). For the other cases, its influence is minimal.

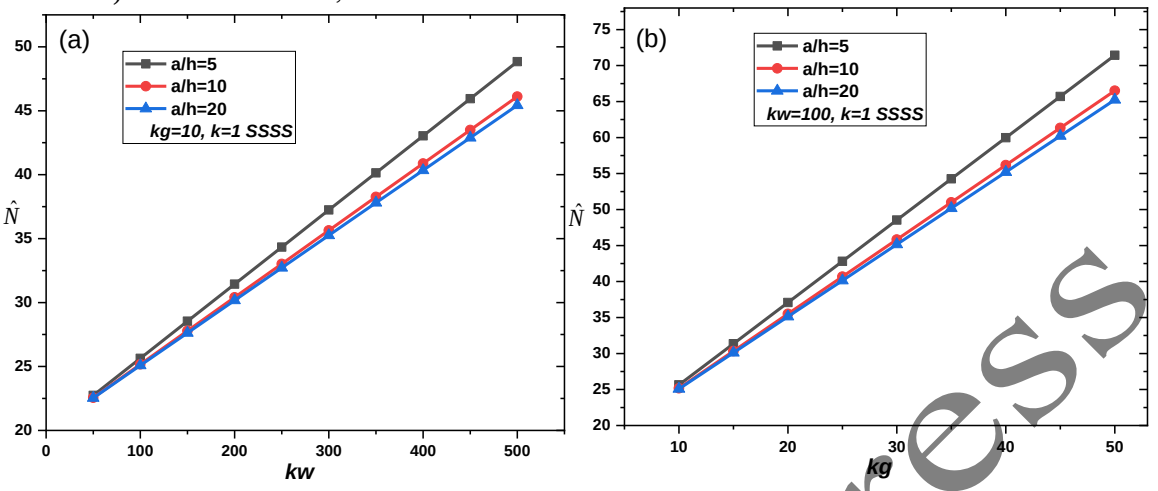

Fig 5. effect of the elastic foundation parameter on the critical buckling load ($\hat{N}$) for a simply supported FG plate (a) Effect of Winkler parameter, (b) Effect of Pasternak parameter (UVL, $\Omega_0 = 0$)

Figure 6 shows the variation of the critical buckling load as a function of the volume fraction index for the first three modes. The highest critical buckling loads correspond to the case of "*k=0*", i.e. the case of an isotropic plate made entirely of ceramic. The increase in the values of the index *k*, which corresponds to the reduction in the quantity of ceramic in the plate and therefore a reduction in rigidity, leads to a reduction in the critical buckling load. In addition, as can be seen in this figure, the modes have a great influence on the critical buckling loads. Indeed, the lowest critical buckling loads are obtained for mode (1,1). Then, for a value of *k=0*, the critical load increases by about 300% for mode (1,2) and by 900% for mode (1,3). This increase tends to decrease with increasing values of the k index.

In addition, the presence of an elastic foundation causes an increase in the stiffness of the plate and consequently an increase in the critical buckling loads.

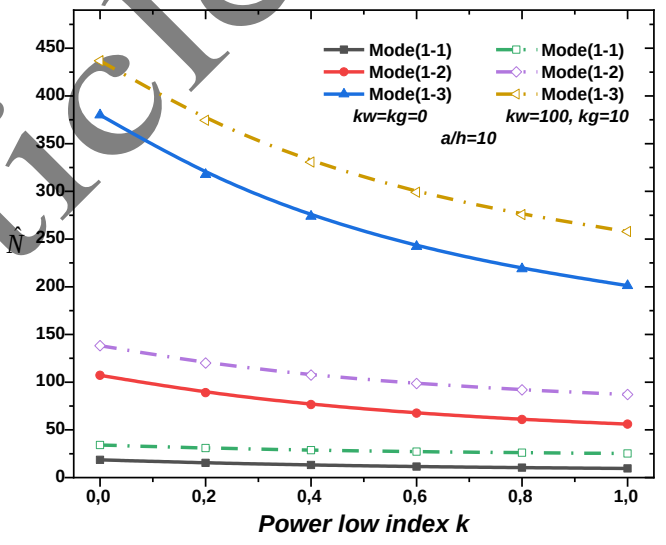

Fig 6. variation of the critical buckling load ($\hat{N}$) versus the power-law index of simply supported FG plate with & without elastic foundations and for different modes (UVL, $\Omega_0 = 0$)

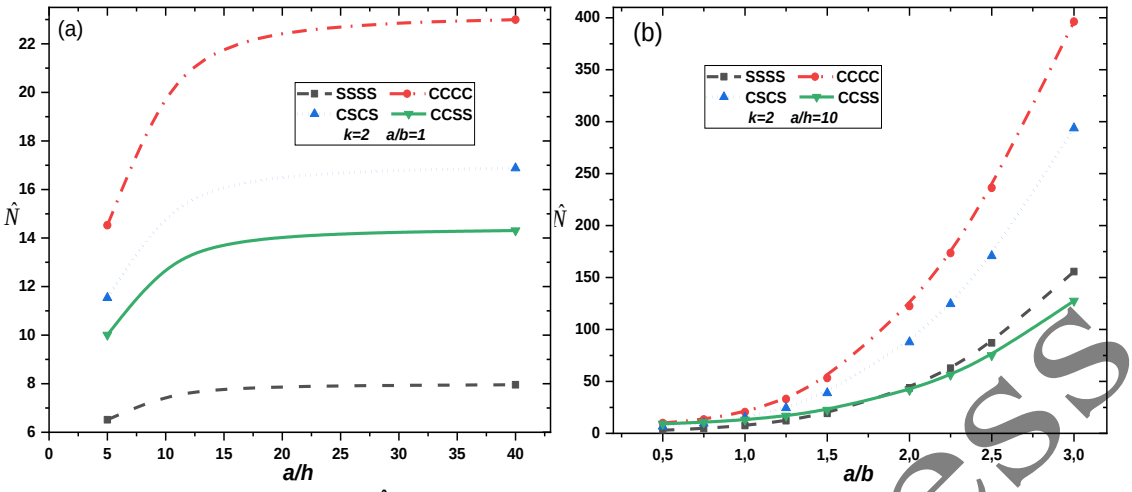

Fig 7.Variation of the of critical buckling load ($\hat{N}$) of FG plate resting on elastic foundation versus: a)-side-to-thickness ratio "a/h" and b) aspect ratio "a/b", under different boundary conditions.

Figure 7 (a) and (b) depicts respectively the variation of critical buckling load ($\hat{N}$) versus the side-to-thickness ratio "*a/h*" and the aspect ratio "*a/b*" for FG plate resting on elastic foundation under different boundary conditions. It is seen that the maximum values of the critical buckling loads are obtained for the clamped boundary condition (CCCC) and this for the two figures. This can be explained by the fact that the embedding of the plate on these four edges offers it additional rigidity and consequently the critical buckling loads increase. The lowest critical buckling loads are obtained for the SSSS condition and the other edge conditions, namely CCSS and CSCS, lie between the first two.

In addition, it was found in Figure 7b that the critical buckling loads increase with the geometry ratio "*a/b"*. Therefore, in order to have a high critical buckling load, it is better to have a rectangular plate geometry than a square one.

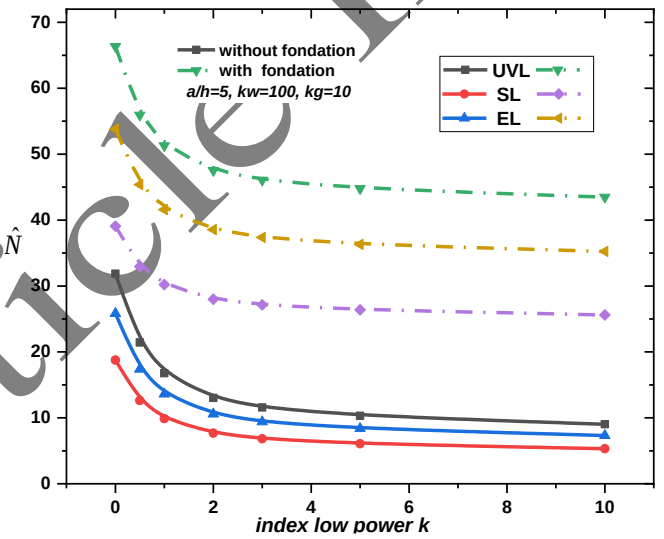

Fig 8. Comparison of the critical buckling loads ($\hat{N}$)for different types of in-plane load of FG plate simply supported with and without elastic foundations ($\Omega_0 = 1$)

To examine the influence of the in-plane compressive load on the critical buckling load of FG simply supported plate with and without elastic foundation; the variation of critical buckling load versus the volume fraction index "*k*" is displayed in figure 8.

As it can be seen from this figure, plate under subjected to UVL always has a maximum critical buckling load than any other load and this with or without an elastic foundation.

The effect of the three Kerr foundation parameters on the critical buckling load of a simply supported FG plate is shown in figure 9. The results are given for three values of the *a/h* ratio (5, 10 and 20). According to this figure, the critical buckling load is increased by increasing the parameters *Ks* and *Ku*, while it is decreased by increasing the parameter *Kl*, regardless of the side-to-thickness ratio "*a/h*".

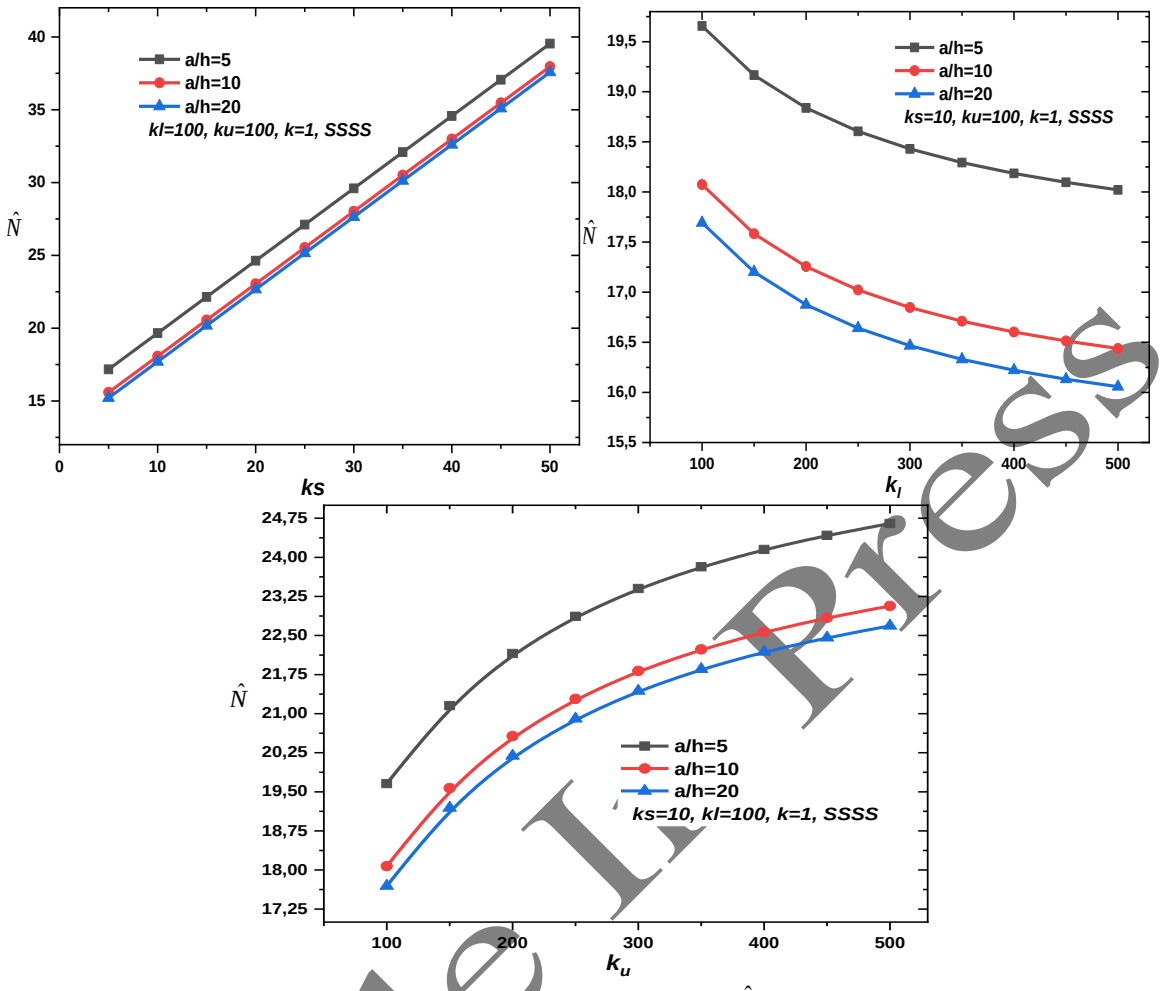

Fig 9. effect of the three parameter of Kerr foundation on the critical buckling load ($\hat{N}$) of FG square simply supported plate (UVL, a/h =5, 10, 20)

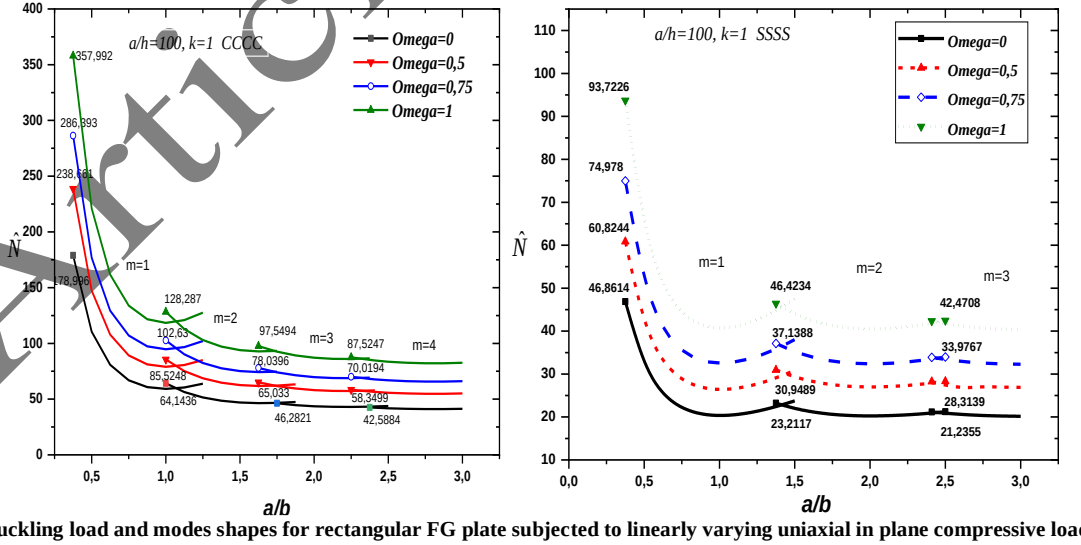

Fig 10.Buckling load and modes shapes for rectangular FG plate subjected to linearly varying uniaxial in plane compressive load (without elastic foundation)

Figure 10 shows that the critical buckling loads are obtained for the case of a triangular compressive load $(\Omega_0 = 1)$, the lowest for a uniformly distributed load $(\Omega_0 = 0)$. The trapezoidal loading $(0 \prec \Omega_0 \prec 1)$ gives

critical buckling loads between the first two types for both boundary conditions (SSSS and CCCC). In addition, the curves indicate values of *a/b* ratio in which mode transition occurs.

5. Conclusion

In the present article, the buckling response of FG plate resting on Kerr/Pasternak/Winkler foundation and subjected to in-plane loading is studied and analyzed. The formulation used in this work is based on quasi-3D theory which takes into account the stretching effect. Three types of elastic foundations have been used such as Kerr, Winkler, and Pasternak and several boundary conditions are considered. The equations of motion have been derived from Hamilton's principle. The critical buckling loads are obtained after solving the problem by Navier solution. A parametric study has been carried out to highlight the effect of the material grading indexes, in-plan compressive load, elastic foundation parameters, boundary conditions and other parameters on critical buckling loads of FG plate on elastic foundation.

According to the results of the study, the followings can be drawn:

- The triangular load gives the highest critical loads compared to the other load cases,
- An FG plate with a CCCC boundary condition gives the highest critical buckling loads compared to other boundary conditions,
- The highest critical buckling loads are given by isotropic plate made entirely of ceramic. The increase in the values of the index *k*, leads to a reduction in the critical buckling load,
- Elastic foundation increases the critical buckling loads of the plate regardless of its composition,
- A rectangular FG plate gives higher critical buckling loads than a square one.

Although this document deals with the analysis of buckling, the formulation used can be extended for the analysis of other types of materials and other models [54-60].

Statements and Declarations

The author(s) declared no potential conflicts of interest with respect to the research, authorship, and/or publication of this article.

References

[1] A. Naderi, A. Saidi, An analytical solution for buckling of moderately thick functionally graded sector and annular sector plates, *Archive of Applied Mechanics,* Vol. 81, pp. 809-828, 2011.

[2] V. R. Kar, S. K. Panda, Nonlinear flexural vibration of shear deformable functionally graded spherical shell panel, *Steel Compos. Struct,* Vol. 18, No. 3, pp. 693-709, 2015.

[3] M. Avcar, Free vibration of imperfect sigmoid and power law functionally graded beams, *Steel and Composite Structures, An International Journal,* Vol. 30, No. 6, pp. 603-615, 2019.

[4] A. Selmi, Exact solution for nonlinear vibration of clamped-clamped functionally graded buckled beam, *Smart Structures and Systems, An International Journal,* Vol. 26, No. 3, pp. 361-371, 2020.

[5] M. Vinyas, On frequency response of porous functionally graded magneto-electro-elastic circular and annular plates with different electro-magnetic conditions using HSDT, *Composite Structures,* Vol. 240, pp. 112044, 2020.

[6] E. Madenci, A refined functional and mixed formulation to static analyses of fgm beams, *Structural Engineering and Mechanics, An Int'l Journal,* Vol. 69, No. 4, pp. 427-437, 2019.

[7] M. A. Attia, On the mechanics of functionally graded nanobeams with the account of surface elasticity, *International Journal of Engineering Science,* Vol. 115, pp. 73-101, 2017.

[8] M. S. Sari, S. Ghaffari, S. Ceballes, A. Abdelkefi, Buckling response of functionally graded nanoplates under combined thermal and mechanical loadings, *Journal of Nanoparticle Research,* Vol. 22, pp. 1-21, 2020.

[9] M. Taczała, R. Buczkowski, M. Kleiber, Nonlinear buckling and post-buckling response of stiffened FGM plates in thermal environments, *Composites Part B: Engineering,* Vol. 109, pp. 238-247, 2017.

[10] P. T. Thang, T. Nguyen-Thoi, D. Lee, J. Kang, J. Lee, Elastic buckling and free vibration analyses of porous-cellular plates with uniform and non-uniform porosity distributions, *Aerospace science and technology,* Vol. 79, pp. 278-287, 2018.

[11] D. Chen, J. Yang, S. Kitipornchai, Buckling and bending analyses of a novel functionally graded porous plate using Chebyshev-Ritz method, *Archives of Civil and Mechanical Engineering,* Vol. 19, No. 1, pp. 157-170, 2019.

[12] W. G. Abdelrahman, Effect of material transverse distribution profile on buckling of thick functionally graded material plates according to TSDT, *Structural Engineering and Mechanics, An Int'l Journal*, Vol. 74, No. 1, pp. 83-90, 2020.

[13] A. Cutolo, V. Mallardo, M. Fraldi, E. Ruocco, Third-order nonlocal elasticity in buckling and vibration of functionally graded nanoplates on Winkler-Pasternak media, *Annals of Solid and Structural Mechanics*, Vol. 12, pp. 141-154, 2020.

[14] V. N. Van Do, K.-H. Chang, C.-H. Lee, Post-buckling analysis of FGM plates under in-plane mechanical compressive loading by using a mesh-free approximation, *Archive of Applied Mechanics*, Vol. 89, pp. 1421-1446, 2019.

[15] T. I. Thinh, T. M. Tu, T. H. Quoc, N. V. Long, Vibration and buckling analysis of functionally graded plates using new eight-unknown higher order shear deformation theory, *Latin American Journal of Solids and Structures*, Vol. 13, pp. 456-477, 2016.

[16] S.-C. Yi, L.-Q. Yao, B.-J. Tang, A novel higher-order shear and normal deformable plate theory for the static, free vibration and buckling analysis of functionally graded plates, *Mathematical Problems in Engineering*, Vol. 2017, 2017.

[17] V. R. Kar, S. K. Panda, Post-buckling behaviour of shear deformable functionally graded curved shell panel under edge compression, *International Journal of Mechanical Sciences*, Vol. 115, pp. 318-324, 2016.

[18] V. Singh, R. Kumar, S. Patel, N. Roy, Nonlinear response and buckling of imperfect plates under in-plane pulse forces: A semi-analytical investigation, *Iranian Journal of Science and Technology, Transactions of Mechanical Engineering*, Vol. 46, No. 3, pp. 633-648, 2022.

[19] Z. Kolakowski, L. Czechowski, Non-linear stability of the in-plane functionally graded (FG) plate, *Composite Structures*, Vol. 214, pp. 264-268, 2019.

[20] P. H. Cong, T. M. Chien, N. D. Khoa, N. D. Duc, Nonlinear thermomechanical buckling and post-buckling response of porous FGM plates using Reddy's HSDT, *Aerospace Science and Technology*, Vol. 77, pp. 419-428, 2018.

[21] A. Tamrabet, C. Mourad, N. Ali Alselami, A. Menasria, B. Mamen, A. Bouhadra, Efficient Kinematic model for Stability Analysis of Imperfect Functionally Graded Sandwich Plates with Ceramic middle layer and Varied Boundary Edges, *Journal of Computational Applied Mechanics*, 2024.

[22] R. Slimani, A. Menasria, M. Ali Rachedi, C. Mourad, S. Refrafi, A. A. Nimer, A. Bouhadra, B. Mamen, A novel quasi-3D refined HSDT for static bending analysis of porous functionally graded Plates, *Journal of Computational Applied Mechanics*, 2024.

[23] s. Refrafi, a. Boutrid, a. Bouhadra, a. Menasria, b. Mamen, Quasi-3d analytic model for free vibration analysis of simply supported functionally graded plates (ss-fgp).

[24] A. Messaoudi, A. Bouhadra, A. Menasria, B. Mamen, B. Boucham, M. Benguediab, A. Tounsi, M. Al-Osta, Impact of the Shear and Thickness Stretching Effects on the Free Vibrations of Advanced Composite Plates, *Mechanics of Composite Materials*, Vol. 59, No. 5, pp. 1001-1018, 2023.

[25] D. Shahsavari, B. Karami, H. R. Fahham, L. Li, On the shear buckling of porous nanoplates using a new size-dependent quasi-3D shear deformation theory, *Acta Mechanica*, Vol. 229, pp. 4549-4573, 2018.

[26] M. Bodaghi, A. Saidi, Stability analysis of functionally graded rectangular plates under nonlinearly varying in-plane loading resting on elastic foundation, *Archive of Applied Mechanics*, Vol. 81, pp. 765-780, 2011.

[27] S. Singh, S. P. Harsha, Buckling analysis of FGM plates under uniform, linear and non-linear in-plane loading, *Journal of Mechanical Science and Technology*, Vol. 33, pp. 1761-1767, 2019.

[28] M. Mohammadi, A. Farajpour, M. Goodarzi, Numerical study of the effect of shear in-plane load on the vibration analysis of graphene sheet embedded in an elastic medium, *Computational Materials Science*, Vol. 82, pp. 510-520, 2014.

[29] M. Mohammadi, A. Farajpour, M. Goodarzi, F. Dinari, Thermo-mechanical vibration analysis of annular and circular graphene sheet embedded in an elastic medium, *Latin American Journal of Solids and Structures*, Vol. 11, pp. 659-682, 2014.

[30] M. Mohammadi, A. Moradi, M. Ghayour, A. Farajpour, Exact solution for thermo-mechanical vibration of orthotropic mono-layer graphene sheet embedded in an elastic medium, *Latin American Journal of Solids and Structures*, Vol. 11, pp. 437-458, 2014.

[31] M. Mohammadi, M. Safarabadi, A. Rastgoo, A. Farajpour, Hygro-mechanical vibration analysis of a rotating viscoelastic nanobeam embedded in a visco-Pasternak elastic medium and in a nonlinear thermal environment, *Acta Mechanica*, Vol. 227, pp. 2207-2232, 2016.

[32] C. Chu, M. Al-Furjan, R. Kolahchi, A. Farrokhian, A nonlinear Chebyshev-based collocation technique to frequency analysis of thermally pre/post-buckled third-order circular sandwich plates, *Communications in Nonlinear Science and Numerical Simulation*, Vol. 118, pp. 107056, 2023.

[33] M. Al-Furjan, Z. Qi, L. Shan, A. Farrokhian, X. Shen, R. Kolahchi, Nano supercapacitors with practical application in aerospace technology: Vibration and wave propagation analysis, *Aerospace Science and Technology*, Vol. 133, pp. 108082, 2023.

[34] P. Wan, M. Al-Furjan, R. Kolahchi, L. Shan, Application of DQHFEM for free and forced vibration, energy absorption, and post-buckling analysis of a hybrid nanocomposite viscoelastic rhombic plate assuming CNTs' waviness and agglomeration, *Mechanical Systems and Signal Processing*, Vol. 189, pp. 110064, 2023.

[35] M. Al-Furjan, S. Fan, L. Shan, A. Farrokhian, X. Shen, R. Kolahchi, Wave propagation analysis of micro air vehicle wings with honeycomb core covered by porous FGM and nanocomposite magnetostrictive layers, *Waves in Random and Complex Media*, pp. 1-30, 2023.

[36] L. Shan, C. Tan, X. Shen, S. Ramesh, M. Zarei, R. Kolahchi, M. Hajmohammad, The effects of nano-additives on the mechanical, impact, vibration, and buckling/post-buckling properties of composites: A review, *Journal of Materials Research and Technology*, 2023.

[37] C. Chu, L. Shan, M. Al-Furjan, A. Farrokhian, R. Kolahchi, Energy absorption, free and forced vibrations of flexoelectric nanocomposite magnetostrictive sandwich nanoplates with single sinusoidal edge on the frictional torsional viscoelastic medium, *Archives of Civil and Mechanical Engineering*, Vol. 23, No. 4, pp. 223, 2023.

[38] C. Chu, M. Al-Furjan, R. Kolahchi, Energy harvesting and dynamic response of SMA nano conical panels with nanocomposite piezoelectric patch under moving load, *Engineering Structures*, Vol. 292, pp. 116538, 2023.

[39] P. Wan, M. Al-Furjan, R. Kolahchi, Nonlinear flutter response and reliability of supersonic smart hybrid nanocomposite rupture trapezoidal plates subjected to yawed flow using DQHFEM, *Aerospace Science and Technology*, Vol. 145, pp. 108862, 2024.

[40] R. Kolahchi, B. Keshtegar, N.-T. Trung, Optimization of dynamic properties for laminated multiphase nanocomposite sandwich conical shell in thermal and magnetic conditions, *Journal of Sandwich Structures & Materials*, Vol. 24, No. 1, pp. 643-662, 2022.

[41] M. Motezaker, R. Kolahchi, D. K. Rajak, S. Mahmoud, Influences of fiber reinforced polymer layer on the dynamic deflection of concrete pipes containing nanoparticle subjected to earthquake load, *Polymer Composites*, Vol. 42, No. 8, pp. 4073-4081, 2021.

[42] M. H. Hajmohammad, A. Farrokhian, R. Kolahchi, Dynamic analysis in beam element of wave-piercing Catamarans undergoing slamming load based on mathematical modelling, *Ocean Engineering*, Vol. 234, pp. 109269, 2021.

[43] M. Al-Furjan, M. H. Hajmohammad, X. Shen, D. K. Rajak, R. Kolahchi, Evaluation of tensile strength and elastic modulus of 7075-T6 aluminum alloy by adding SiC reinforcing particles using vortex casting method, *Journal of Alloys and Compounds*, Vol. 886, pp. 161261, 2021.

[44] M. Al-Furjan, M. Xu, A. Farrokhian, G. S. Jafari, X. Shen, R. Kolahchi, On wave propagation in piezoelectric-auxetic honeycomb-2D-FGM micro-sandwich beams based on modified couple stress and refined zigzag theories, *Waves in Random and Complex Media*, pp. 1-25, 2022.

[45] M. Al-Furjan, Y. Yang, A. Farrokhian, X. Shen, R. Kolahchi, D. K. Rajak, Dynamic instability of nanocomposite piezoelectric-leptadenia pyrotechnica rheological elastomer-porous functionally graded materials micro viscoelastic beams at various strain gradient higher-order theories, *Polymer Composites*, Vol. 43, No. 1, pp. 282-298, 2022.

[46] M. Al-Furjan, C. Yin, X. Shen, R. Kolahchi, M. S. Zarei, M. Hajmohammad, Energy absorption and vibration of smart auxetic FG porous curved conical panels resting on the frictional viscoelastic torsional substrate, *Mechanical Systems and Signal Processing*, Vol. 178, pp. 109269, 2022.

[47] M. Al-Furjan, L. Shan, X. Shen, R. Kolahchi, D. K. Rajak, Combination of FEM-DQM for nonlinear mechanics of porous GPL-reinforced sandwich nanoplates based on various theories, *Thin-Walled Structures*, Vol. 178, pp. 109495, 2022.

[48] M. Al-Furjan, L. Shan, X. Shen, M. Zarei, M. Hajmohammad, R. Kolahchi, A review on fabrication techniques and tensile properties of glass, carbon, and Kevlar fiber reinforced rolymer composites, *Journal of Materials Research and Technology*, Vol. 19, pp. 2930-2959, 2022.

[49] C. Chu, L. Shan, M. Al-Furjan, M. Zarei, M. Hajmohammad, R. Kolahchi, Experimental study for the effect of hole notched in fracture mechanics of GLARE and GFRP composites subjected to quasi-static loading, *Theoretical and Applied Fracture Mechanics*, Vol. 122, pp. 103624, 2022.

[50] M. Al-Furjan, R. Kolahchi, L. Shan, M. Hajmohammad, A. Farrokhian, X. Shen, Slamming impact induced hydrodynamic response in wave-piercing catamaran beam elements with controller, *Ocean Engineering*, Vol. 266, pp. 112908, 2022.

[51] F. Achouri, S. Benyoucef, F. Bourada, R. B. Bouiadjra, A. Tounsi, Robust quasi 3D computational model for mechanical response of FG thick sandwich plate, *Struct. Eng. Mech*, Vol. 70, No. 5, pp. 571-589, 2019.

[52] M. A. A. Meziane, H. H. Abdelaziz, A. Tounsi, An efficient and simple refined theory for buckling and free vibration of exponentially graded sandwich plates under various boundary conditions, *Journal of Sandwich Structures & Materials,* Vol. 16, No. 3, pp. 293-318, 2014.

[53] M. Mekerbi, S. Benyoucef, A. Mahmoudi, A. Tounsi, A. A. Bousahla, S. Mahmoud, Thermodynamic behavior of functionally graded sandwich plates resting on different elastic foundation and with various boundary conditions, *Journal of Sandwich Structures & Materials,* Vol. 23, No. 3, pp. 1028-1057, 2021.

[54] S. A. Asiri, Ş. D. Akbaş, M. A. Eltaher, Damped dynamic responses of a layered functionally graded thick beam under a pulse load, *Structural Engineering and Mechanics, An Int'l Journal,* Vol. 75, No. 6, pp. 713-722, 2020.

[55] A. Boulal, T. Bensattalah, A. Karas, M. Zidour, H. Heireche, E. A. Bedia, Buckling of carbon nanotube reinforced composite plates supported by Kerr foundation using Hamilton's energy principle, *Structural Engineering and Mechanics, An Int'l Journal,* Vol. 73, No. 2, pp. 209-223, 2020.

[56] M. A. Eltaher, Ş. D. Akbaş, Transient response of 2D functionally graded beam structure, *Structural Engineering and Mechanics, An Int'l Journal,* Vol. 75, No. 3, pp. 357-367, 2020.

[57] P. V. Katariya, S. K. Panda, Numerical analysis of thermal post-buckling strength of laminated skew sandwich composite shell panel structure including stretching effect, *Steel and Composite Structures, An International Journal,* Vol. 34, No. 2, pp. 279-288, 2020.

[58] M. Yaylacı, Numerical analysis of the receding contact problem of two bonded layers resting on an elastic half plane, *Structural Engineering and Mechanics, An Int'l Journal,* Vol. 72, No. 6, pp. 775-783, 2019.

[59] K. Mehar, S. K. Panda, Nonlinear deformation and stress responses of a graded carbon nanotube sandwich plate structure under thermoelastic loading, *Acta Mechanica,* Vol. 231, No. 3, pp. 1105-1123, 2020.

[60] O. Civalek, M. Jalaei, Buckling of carbon nanotube (CNT)-reinforced composite skew plates by the discrete singular convolution method, *Acta Mechanica,* Vol. 231, pp. 2565-2587, 2020.